

A practical Visual Servo Control for a Unmanned Aerial Vehicle

Nicolas Guenard

CEA/LIST

Fontenay-aux-roses, France

Email: guenardn@zoe.cea.fr

Tarek Hamel

I3S-CNRS

Nice-Sophia Antipolis, France

Email: thamel@i3s.unice.fr

Robert Mahony

Dep. of Eng., Australian National University,
ACT, 0200, AUSTRALIA.

Email: mahony@ieee.org

Abstract— An image-based visual servo control is presented for an Unmanned aerial vehicle (UAV) capable of stationary or quasi-stationary flight. The proposed control design addresses visual servo of ‘eye-in-hand’ type systems. The control of the position and orientation dynamics are decoupled using a visual error based on a spherical centroid data, along with estimation of the gravitational inertial direction. The error used compensates for the poor conditioning of the Jacobian matrix seen in earlier work in this area by introducing a non-homogeneous gain term adapted to the visual sensitivity of the error measurements. A nonlinear controller is derived for the full dynamics of the system. Experimental results on an experimental UAV known as an X4-flyer made by the French Atomic Energy Commission (CEA) demonstrate the robustness and performance of the proposed control strategy.

I. INTRODUCTION

Visual servo algorithms have been extensively developed in the robotics field over the last ten years [10], [21]. Most visual servo control has been developed for serial-link robotic manipulators with the camera typically mounted on the end-effector [13]. Visual servo systems may be divided into two main classes [17]; *position-based visual servo* (PBVS) control or *image-based visual servo* (IBVS) control. Position based visual servo control involves reconstruction of the target pose with respect to the robot and results in a Cartesian motion planning problem. This approach requires an accurate 3D model of the target, is sensitive to camera calibration errors and displays a tendency for image features to leave the camera field of view during the task evolution. Image-based visual servo control treats the problem as one of controlling features in the image plane, such that moving features to a goal configuration implicitly results in the task being accomplished [10]. Feature errors are mapped to actuator inputs via the inverse of an image Jacobian matrix. There are a wide range of features that have been considered including; points, lines, circles and image moments. Different features lead to different closed-loop response and there has been important research into optimal selection of features and partitioned control where some degrees of freedom are controlled visually and others by a second sensor modality [14], [5]. IBVS avoids many of the robustness and calibration problems associated with PBVS, however, it has its own problems [6]. Foremost in the classical approach is a requirement

to estimate the depth of each feature point in the visual data. Various approaches have been reported including; estimation via partial pose estimation [17], adaptive control [19] and estimation of the image Jacobian using quasi-Newton techniques [20]. More recently, there has been considerable interest in hybrid control methods whereby translational and rotational control are treated separately [17], [9]. Hybrid methods, however, share with the PBVS approach a difficulty to keep all image features within the camera’s field of view. Contemporary work [18], [7] aims to address these issues.

Most existing IBVS approaches was developed for serial-link robotic manipulators. For this kind of robot (or fully-actuated systems) the system dynamics are dominated using high gain and the visual servo control is solved directly for the system kinematics [10]. There are very few integrated IBVS control designs for fully dynamic system models [24], [3] and even fewer that deal with under-actuated dynamic models. The key problem in applying the classical visual servo control approach lies in the highly coupled form of the image Jacobian. Much of the existing work in visual servo control of aerial robots (and particularly autonomous helicopters) have used pose based visual servo methodology [1], [22]. Prior work by the authors [12] proposed a theoretical IBVS approach for a class of under actuated-dynamics without considering the practical aspect.

In this paper the practical aspect of an image-based visual servo control for a UAV, capable of stationary or quasi-stationary flight, is considered. The model considered is that of an ‘eye-in-hand’ type configuration, where the camera is attached to the airframe of the UAV. The approach taken is based on recent work by the authors [12] for which the dynamics of the image features have certain passivity-like properties. A new visual error term is considered that improves the conditioning of the image Jacobian. The initial analysis is undertaken for the kinematic response of the system, the normal visual servo framework, and shows that the resulting image Jacobian is well conditioned. Following this, a non-linear control is developed for stabilisation of the full dynamics of the UAV. Experimental results are obtained on an experimental X4-flyer UAV system developed within CEA capable of stationary and quasi-stationary flight. The closed-loop visual

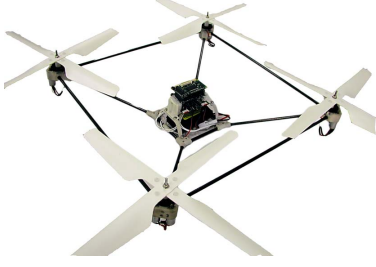


Fig. 1: The X4-flyer UAV

servo control demonstrates the expected performance and robustness of the proposed control.

The paper is arranged into six sections. Section II presents the fundamental equations of motion for an X4-flyer UAV. Section III presents the proposed choice of image features. Section IV provides a Kinematic control design for the translational motion. Section V extends the control to the full dynamics of the system. Section VI presents experimental results obtained on the experimental X4-flyer (fig. 1).

II. A GENERAL UAV DYNAMIC MODEL

In this section, we derive equations of motion for a UAV in quasi-stationary flight conditions. Let $\mathcal{I} = \{e_1, e_2, e_3\}$ denote a right-hand inertial or world frame such that E_z denotes the vertical direction downwards into the earth. Let $\xi = (x, y, z)$ denote the position of the centre of mass of the object in the inertial frame \mathcal{I} . Let $\mathcal{A} = \{E_1^a, E_2^a, E_3^a\}$ be a (right-hand) body fixed frame. The orientation of the airframe is given by a rotation $R : \mathcal{A} \rightarrow \mathcal{I}$, where $R \in SO(3)$ is an orthogonal rotation matrix.

Let $V \in \mathcal{A}$ denote the linear velocity and $\Omega \in \mathcal{A}$ denote the angular velocity of the camera both expressed in the camera frame. Let m denote the mass of the rigid object and let $\mathbf{I} \in \mathbb{R}^{3 \times 3}$ be the constant inertia matrix around the centre of mass (expressed in the body fixed frame \mathcal{A}). Newton's equations of motion yield the following dynamic model for the motion of a rigid object:

$$\dot{\xi} = RV \quad (1)$$

$$m\dot{V} = -m\Omega \times V + F \quad (2)$$

$$\dot{R} = R \text{sk}(\Omega), \quad (3)$$

$$\mathbf{I}\dot{\Omega} = -\Omega \times \mathbf{I}\Omega + \Gamma. \quad (4)$$

where F is the vector forces and Γ is the vector torques. The notation $\text{sk}(\Omega)$ denotes the skew-symmetric matrix such that $\text{sk}(\Omega)v = \Omega \times v$ for the vector cross-product \times and any vector $v \in \mathbb{R}^3$.

For a typical UAV capable of stationary or quasi-stationary flight, the vector force F is defined as follows:

$$F = mgR^T e_3 - T e_3 \quad (5)$$

In the above notation, g is the acceleration due to gravity, and T a scalar input termed the thrust or heave, applied in direction e_3 .

III. CHOICE OF IMAGE FEATURES

A. Kinematics of an image point under spherical projection

Let P be a stationary point target visible to the camera expressed in the camera frame. The image point observed by the camera is denoted p and is obtained by rescaling onto the image surface \mathcal{S} of the camera (cf. Figure 2). Following the approach introduced in [12] we consider a camera with a spherical image plane. Thus,

$$p = \frac{P}{|P|}. \quad (6)$$

Where $|x|$ represents the norm of any vector $x \in \mathbb{R}^n$, $|x| = \sqrt{x^T x}$. The dynamics of an image point for a spherical camera of image surface radius unity are (see [12], [4])

$$\dot{p} = -\Omega \times p - \frac{\pi_p}{|P|} V, \quad (7)$$

where $\pi_p = (I_3 - pp^T)$ is the projection $\pi_p : \mathbb{R}^3 \rightarrow T_p S^2$, the tangent space of the sphere S^2 at the point $p \in S^2$.

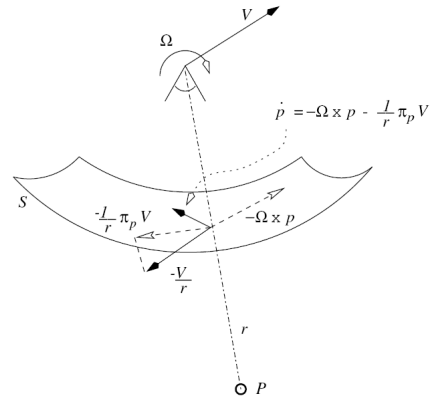


Fig. 2: Image dynamics for spherical camera image geometry.

B. Centroid of a target surface

Consider a point target consisting of N points $\{P_i\}$ with image points $\{p_i\}$. The centroid of a target is defined to be

$$q_0 := \frac{\sum_{i=1}^n p_i}{|\sum_{i=1}^n p_i|} \in S^2$$

In the case that the image is a continuous surface \mathcal{S} on the spherical image plane, one has

$$q_0 := \frac{\int_{p \in \mathcal{S}} p dp}{\left| \int_{p \in \mathcal{S}} p dp \right|}.$$

The centroid measures the centre of mass of the *observed image* in the chosen camera geometry. The centroid depends implicitly on the camera geometry and for a different geometry (such as a camera with perspective projection) the direction of the centroid will be different.

Using centroid information is an old technique in visual servo control [2], [15], [23]. Among the advantages one has that it is not necessary to match observed image

points with desired features as would be necessary in classical image based visual servo control [13], and the calculation of an image centroid is highly robust to pixel noise and can be easily programmed in real-time. The disadvantage of a classical image centroid is that it contains effectively two measurements linked to the direction of centroid with respect to the body-fixed-frame axes of the camera. However, there is certain amount of information regarding the depth of an observed target that may be extracted directly from an un-normalized centroid in the spherical

$$q := \sum_{i=1}^n p_i \in \mathbb{R}^3. \quad (8)$$

Intuitively, as the camera approaches the geometric centre of the target points the observed image points spread out around the camera and (assuming the camera has a wide range of view such as is obtained by a panoramic camera) the un-normalized centroid converges to zero. Conversely, as the camera moves away from the geometric centre of the target points, all the observe image points converge towards each other, and q converges to a vector that has norm N and points towards the target.

If the target is a discrete target, for a point target comprising a finite number of image points the kinematics of the image centroid are easily verified to be

$$\dot{q} = -\Omega \times q - QV, \quad (9)$$

where

$$Q = \sum_{i=1}^{i=n} \frac{\pi p_i}{r(P_i)}. \quad (10)$$

C. Image based errors

Note that the centroid of an image is insufficient information to position the full pose of the camera. Additional information exists in the second and higher order moments. Indeed, the zero order moment provides only depth information, the first order moments provide information on lateral displacement, the second order moments provide information on relative orientation of the camera with respect to the target. If purely centroid information is used then additional image or inertial information must be incorporated into the error to fully specify the camera pose. In this paper we will augment the image information with inertial information acquired from a standard inertial measurement unit (IMU) used in most small scale UAVs.

Formally, let $b \in \mathcal{I}$ denote the desired inertial direction for the visual feature. The norm of b encodes the effective depth information for the desired limit point. Define

$$q^* := R^T b \in \mathcal{A}$$

to be the desired target vector expressed in the camera fixed frame. The orientation matrix R is estimated from filtered data acquired on a strap down IMU on the vehicle. Since $q^* \in \mathcal{A}$, it inherits dynamics from the motion of the camera

$$\dot{q}^* = -\Omega \times q^*.$$

The natural image based error is the difference between the measured centroid and the target vector expressed in the camera frame

$$\delta := q - q^*. \quad (11)$$

The image error kinematics are

$$\dot{\delta} = -\Omega \times \delta - QV \quad (12)$$

To regulate the full pose of the camera using a fully-actuated kinematic system (such a robotic manipulator) it is necessary to consider an additional error criterion for the orientation. Note that any rotation of the camera that alters the observed image centroid may be controlled using centroid information [16]. However, the image centroid is invariant under rotation around the axis of the centroid. Thus, the best that can be achieved using the centroid feature is to orient the camera such that the image centroid lies in a desired direction. To control the remaining degrees of freedom one must use additional information; either from the image or a prior inertial direction [16].

For the class of under-actuated dynamic systems considered it is physically necessary to use the attitude dynamics to control the orientation of the force input to the linear dynamics in order to stabilise the position of the system. It is physically impossible to separately stabilise the attitude and position of the camera. The error criterion chosen regulates only the position of the rigid body and the orientation regulation is derived as a consequence of the system dynamics.

IV. KINEMATIC CONTROL DESIGN TRANSLATION MOTION

In this section a Lyapunov control design is given for the translational motion based on the visual error Eq. 12.

Define a storage function S

$$S = \frac{1}{2} |\delta|^2 \quad (13)$$

Taking the time derivative of S and substituting for Eq. 12, yields

$$\dot{S} = -\delta^T QV \quad (14)$$

Note that Eq. 14 is independent of the angular velocity Ω .

The matrix $Q > 0$ is not exactly known, however, it is known to be positive definite and its maximal eigenvalue must satisfy

$$\|Q\| \leq \sum_{i=1}^{i=n} \frac{1}{r_i}. \quad (15)$$

where r_i denotes the relative depth of the i th image point. Thus, a simple choice

$$V = k_\delta \delta, \quad k_\delta > 0$$

is sufficient to stabilise S . Indeed, by substituting the control input V by its expression in Eq. 14, one obtains

$$\dot{S} = -k_\delta \delta^T Q \delta$$

Since Q is a positive definite matrix, classical Lyapunov theory guarantees that δ converges exponentially to zero.

Note that the lower bound on $\|Q\|$ becomes singular as the range between the camera and the target increases to infinity. The eigenvalues of the matrix $\|Q\|$ are generally ill conditioned

$$\lambda_{\min}(Q) \ll \lambda_{\max}(Q).$$

Convergence rates of the components of the error δ depend on the eigenvalues of q . As a consequence the natural control $V = k_\delta \delta$ leads to poor asymptotic conditioning of the closed-loop system.

A. Kinematic compensation of the control gain for sensitivity.

A number of different approaches have been proposed to compensate the poor conditioning of the Jacobian matrix Q and to improve performance of the closed-loop system [4]. In earlier work, only the kinematic model was studied and the dynamics of the system was not considered in the control design. In this paper, we propose a modification of the visual error term to improve the conditioning of the Jacobian matrix Q in the neighborhood of the set point q^* preserving the passivity-like properties and allowing control design for the full dynamics of the system.

At the set point, the Jacobian matrix Q display two eigenvalues of comparable magnitude and one eigenvalue, associated with the direction q^* , that is an order of magnitude smaller. To deal with this ill conditioning two new error terms are introduced:

$$\delta_{11} = q_0^* \times q, \quad \delta_{12} = q_0^{*T} \delta, \quad q_0^* = \frac{q^*}{|q^*|}$$

Deriving δ_1 and δ_2 , it follows

$$\begin{aligned} \dot{\delta}_{11} &= -\text{sk}(\Omega)\delta_1 - \text{sk}(q_0^*)QV \\ \dot{\delta}_{12} &= -q_0^{*T}QV \end{aligned}$$

where sk denotes the operator $\text{sk} : \mathbb{R}^3 \rightarrow \mathbb{R}^{3 \times 3}$ such that $\text{sk}(v)$ is skew symmetric and $\text{sk}(v)w = v \times w$ for all vectors $v, w \in \mathbb{R}^3$.

Lemma 4.1: Consider the system defined by Eq. 12 and let $k, \lambda > 0$ be two positive constants. Assume that the image remains in the camera field of view for all time. Then, the closed loop system Eq. 12 based on the following control Eq. 16

$$V = k(-\text{sk}(q_0^*) + \lambda q_0^* q_0^{*T})(\delta_{11} + \lambda q_0^* \delta_{12}), \quad (16)$$

exponentially stabilises the visual error δ .

Proof:

Define

$$S_1 = \frac{1}{2}|\delta_{11}|^2 + \lambda^2|\delta_{12}|^2$$

It is straightforward to verify that

$$S_1 = \frac{1}{2}|\delta_{11} + \lambda q_0^* \delta_{12}|^2 = \frac{1}{2}\delta_1^2$$

Deriving S_1 and substituting the control input V by its expression yields

$$\dot{S}_1 = -k\delta_1^T H \delta_1$$

where

$$H = A(q_0^*)QA(q_0^*)^T, \quad A(q_0^*) = \text{sk}(q_0^*) + \lambda q_0^* q_0^{*T} \quad (17)$$

Since Q is positive definite matrix and $A(q_0^*)$ a non singular matrix, $H > 0$ and therefore δ_1 converges exponentially to zero.

Due to the decoupling between δ_{11} and δ_{12} and the decrease of the storage function S_1 towards zero guarantee the exponential convergence of the of the error δ to zero. ■

Note that the best choice of the control gain λ affecting the direction of the desired feature q^* could be characterized by the following constraint:

$$H \cong I$$

where the symbol \cong means ‘‘equality up to a multiplicative constant’’.

V. CONTROL DESIGN FOR THE FULL DYNAMICS OF THE SYSTEM

As discussed above, the matrix H (Eq. 17) remains unknown but well conditioned in a large neighborhood around the desired position and the above choice of the velocity V , if it were available as a control input (kinematic control), is sufficient to stabilise S_1 . Note, however, that to deal with the full dynamics of the considered system, the velocity V cannot be used as control input. In this situation a control design based on backstepping procedure is proposed.

With this choice, one has

$$\dot{\delta}_1 = -\text{sk}(\Omega)\delta_1 - \frac{k_1}{m}H\delta_1 - \frac{k_1}{m}H\delta_2 \quad (18)$$

where δ_2 defines the difference between the desired ‘virtual control’ choosing as kinematic control (Eq. 16) and the true velocity

$$\delta_2 := \frac{m}{k_1}A(q_0^*)^{-T}V - \delta_1 \quad (19)$$

and will form an error term to stabilise the translational dynamics. With the above definitions one has

$$\dot{S}_1 = -\frac{k_1}{m}\delta_1^T H \delta_1 - \frac{k_1}{m}\delta_1^T H \delta_2 \quad (20)$$

Noting that

$$A(q_0^*)^{-T} = \text{sk}(q_0^*) + \frac{1}{\lambda}q_0^* q_0^{*T},$$

deriving δ_2 and recalling Eqn’s 2 and 18, it yields

$$\dot{\delta}_2 = -\text{sk}(\Omega)\delta_2 + \frac{k_1}{m}H\delta_1 + \frac{k_1}{m}H\delta_2 + \frac{1}{k_1}A(q_0^*)^{-T}F \quad (21)$$

Let S_2 be the second storage function gathering the translational dynamics used for this control algorithm

$$S_2 = \frac{1}{2}|\delta_1|^2 + \frac{1}{2}|\delta_2|^2 \quad (22)$$

Taking the derivative of S_2 it follows that

$$\begin{aligned} \dot{S}_2 = & -\frac{k_1}{m}\delta_1^T H\delta_1 + \frac{k_1}{m}\delta_2^T H\delta_2 \\ & + \frac{1}{k_1}\delta_2^T A(q_0^*)^{-T} F \end{aligned} \quad (23)$$

The positive definite matrix $H = A(q_0^*)QA(q_0^*)^T$ is well conditioned but is not exactly known, however, there are upper and lower bounds on the eigenvalues of H in the neighborhood of the desired position. Thus, choosing

$$F := -\frac{k_1^2 k_2}{m} A(q_0^*)^T \delta_2, \quad (24)$$

where $k_2 > \lambda_{\max}(H) = \max\{\lambda_{\max}(Q), \lambda^2 \lambda_{\min}(Q)\}$, is sufficient to stabilise the translational dynamics. Since the rigid body system considered is under-actuated, the force input F is unable to assign the desired dynamics directly.

It is necessary to use the above definition as virtual force inputs in a further stage of the backstepping procedure. Set

$$F^v := -\frac{k_1^2 k_2}{m} \delta_2. \quad (25)$$

A new error term δ_3 is defined to measure the scaled difference between the virtual and the true force inputs. It is introduced to deal with the attitude dynamics constrained by the main objective δ_1 :

$$\delta_3 := \frac{m}{k_1^2 k_2} A(q_0^*)^{-T} F + \delta_2. \quad (26)$$

The derivative of δ_2 Eq. 21 becomes:

$$\dot{\delta}_2 = -\text{sk}(\Omega)\delta_2 + \frac{k_1}{m}H\delta_1 - \frac{k_1}{m}(k_2 I_3 - H)\delta_2 + \frac{k_1}{m}k_2\delta_3, \quad (27)$$

and the derivative of the second storage function is now

$$\dot{S}_2 = -\frac{k_1}{m}\delta_1^T H\delta_1 - \frac{k_1}{m}\delta_2^T (k_2 I_3 - H)\delta_2 + \frac{k_1}{m}k_2\delta_2^T \delta_3 \quad (28)$$

Deriving δ_3 and recalling Eq. 21, yields

$$\begin{aligned} \dot{\delta}_3 = & -\text{sk}(\Omega)\delta_3 + \frac{k_1}{m}H\delta_1 - \frac{k_1}{m}(k_2 I_3 - H)\delta_2 + \frac{k_1}{m}k_2\delta_3 \\ & + \frac{m}{k_1^2 k_2} A(q_0^*)^{-T} \left(\dot{F} + \text{sk}(\Omega)F \right) \end{aligned} \quad (29)$$

Recalling Eq. 5, the full vectorial term $\left(\dot{F} + \text{sk}(\Omega)F \right)$ is explicitly given by:

$$\left(\dot{F} + \text{sk}(\Omega)F \right) = \begin{pmatrix} 0 & T & 0 \\ -T & 0 & 0 \\ 0 & 0 & 1 \end{pmatrix} \begin{pmatrix} \Omega_1 \\ \Omega_2 \\ \dot{T} \end{pmatrix} \quad (30)$$

Proposition 5.1: Consider \dot{T} as control input of the thrust T and (Ω_1, Ω_2) as control input of the attitude direction associated with a high gain control to recover the control torques, then choosing

$$\frac{m}{k_1^2 k_2} \left(\dot{F} + \text{sk}(\Omega)F \right) := -\frac{(k_1 k_2 + k_3)}{m} A(q_0^*)^T \delta_3 \quad (31)$$

for $k_3 > 0$, exponentially stabilises δ_1 to zero and ensures the exponential convergence of the attitude direction $R^T e_3$ towards e_3 .

Proof: Let \mathcal{L} be a Lyapunov candidate function defined by

$$\mathcal{L} = \frac{1}{2}|\delta_1|^2 + \frac{1}{2}|\delta_2|^2 + \frac{1}{2}|\delta_3|^2 \quad (32)$$

Taking the derivative of \mathcal{L} and recalling Eq. 29 one obtains

$$\begin{aligned} \dot{\mathcal{L}} = & -\frac{k_1}{m}\delta_1^T H\delta_1 - \frac{k_1}{m}\delta_2^T (k_2 I_3 - H)\delta_2 \\ & - \frac{k_1}{m}\delta_3^T H\delta_1 - \frac{k_1}{m}\delta_3^T (k_2 I_3 - H)\delta_2 - \frac{k_3}{m}\delta_3^T \delta_3 \end{aligned}$$

Completing the square four times to dominate the cross terms, it may be verified that the choice of control gains given in the theorem ensures that the right-hand side is negative definite in all the error signals δ_i , $i = 1, \dots, 3$. Classical Lyapunov theory ensures converges of $\delta_i \rightarrow 0$.

If the position and linear velocity are regulated then the total external force must be zero, $F = 0$. Recalling Eq. 5 one has

$$R^T e_3 = e_3, \quad T = mg. \quad (33)$$

It follows that any rotation of the aerial vehicle that would affect the orientation of thrust is directly stabilised via the backstepping error δ_3 . ■

Note that the error term δ_3 does not determine the full attitude of the system considered. Pitch and roll components of its attitude are regulated by the errors δ_3 . The yaw rotation around the thrust direction is not stabilised. To stabilise the yaw attitude by means of visual information one needs to use additional error criteria [12]. In the experimental Section VI the yaw rate is controlled by a teleoperation mode via a joystick.

VI. EXPERIMENTAL RESULTS

In this section, experimental results of the above algorithms designed for the full dynamics of the system are presented. The UAV used for the experimentation is an X4-flyer, made by the CEA, (fig. 1) which is a vertical take off and landing vehicle ideally suited for stationary and quasi stationary flight.

A. Prototype description

The CEA's X4-flyer is equipped with a set of four electronic boards (fig. 3b) designed by the CEA. Each electronic board includes a micro-controller and has a particular function. The first board integrates the motor controllers which regulate the rotation speed of the four propellers. The second board integrate an Inertial Measurement Unit (IMU) constituted of 3 low cost MEMS accelerometers, which give the gravity components in the body frame, 3 angular rate sensors and 2 magnetometers. On the third board, a Digital Signal Processing (DSP), running at 150 MIPS, is embedded and performs the control algorithm filtering computations. The final board provides a serial wireless communication between the operator's joystick

and the vehicle. An embedded camera (fig. 3a) with a view angle of 120 pointing directly down, transmits video to a ground station (PC) via a traditional analogical link of 2.4GHz. A Lithium-Polymer battery provides nearly 10 minutes of flight time. The loaded weight of the prototype is about 550g. The images sent by the embedded camera

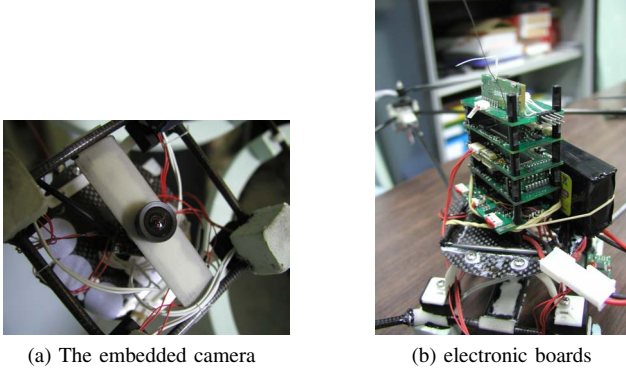


Fig. 3

are received by the ground station at a frequency of 15Hz. In parallel, the X4-flyer sends the inertial data to the station on the ground at a frequency of 9Hz. The data is processed by the ground station PC and incorporated into the control algorithm. Desired orientation velocities and desired thrust rate are generated on the ground station PC and sent to the drone. A key difficulty of the algorithm implementation lies in the relatively large time latency between the inertial data and visual features. For orientation velocities and thrust rate control, an embedded controller in the DSP running at 166Hz, independently ensures its stability from the ground station.

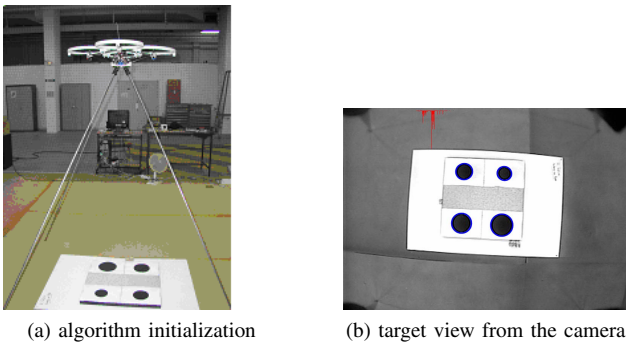


Fig. 4

B. Experiments

1) *target*: The target considered is the four black marks on the vertices of a planar square (cf figure 4b). An algorithm extract the center of the four circles and compute the centroid q (Eq. 8). The characteristics of experimental camera insures that the observed target remains visible if the X4-flyer remains in a ray of 1.5m around the center of the target when this one evolves at an altitude of 1.7m.

The desired image feature b^* is chosen such that the camera set point is located 1.7m above the target:

$$b^* = \begin{pmatrix} 0 \\ 0 \\ 3.96 \end{pmatrix} \quad (34)$$

2) *Initialization*: The initialization of the control algorithm consists in computing the parameter λ to improve the conditioning of the Jacobian matrix Q around the desired position. Initially the X4-flyer is placed at a distance of $z \simeq 1.7m$ above the target ($x \simeq y \simeq 0$), insuring that the Jacobian matrix Q at the desired position is:

$$Q^* \simeq \begin{pmatrix} 2.35 & 0 & 0 \\ 0 & 2.36 & 0 \\ 0 & 0 & 0.056 \end{pmatrix}. \quad (35)$$

Note the ill-conditioning of the matrix Q (the condition number $\rho(Q) = \frac{\lambda_{\max}(Q)}{\lambda_{\min}(Q)} = 42.14$). Since the convergence rates are given by the eigenvalues of $H = A(q_0^*)QA(q_0^*)^T$ rather than of the eigenvalues of Q , choose λ such that $A(q_0^*)QA(q_0^*)^T$ is well conditioned ($\rho(H) \simeq 1$).

$$A(q_0^*) = \begin{pmatrix} 0 & 1 & 0 \\ -1 & 0 & 0 \\ 0 & 0 & \lambda \end{pmatrix}. \quad (36)$$

Consequently, choosing $\lambda = 6.44$, the Jacobian matrix H is well conditioned ($\rho_H \simeq 1$):

$$A(q_0^*)QA(q_0^*)^T \simeq 2.35 \begin{pmatrix} 1 & 0 & 0 \\ 0 & 1 & 0 \\ 0 & 0 & 1 \end{pmatrix}. \quad (37)$$

3) *Results*: During the experiments, the yaw velocity is controlled via the joystick. It has no effect on the proposed control scheme (Eq. 30) and therefore, it has no effect on the convergence of the visual feature. The drone is teleoperated near the target, such that the target marks are visible (about 60 cm in x and y and 2m in z), then the proposed algorithm is initialised. We observe exponential convergence of the three components of the error term δ_1 with a very satisfactory behaviour. Note that various inaccuracies from system modeling and the delays of transmissions generates imprecision smaller than 10cm around the desired position.

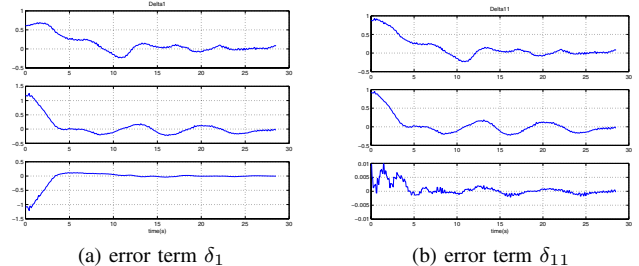


Fig. 5

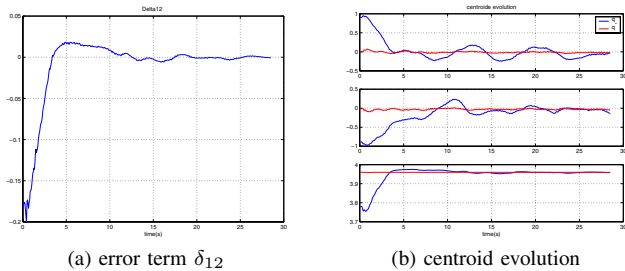


Fig. 6

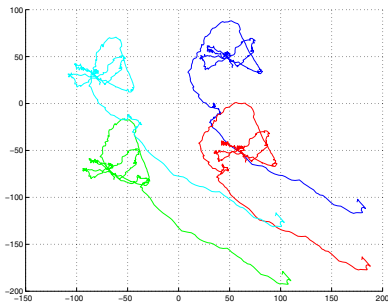


Fig. 7: Trajectory in the image plan of the four black marks

VII. CONCLUSION

In this paper we presented a visual servo control for stabilisation of an X4-flyer UAV. This work is an extension of the recent theoretical work on visual servo control of under-actuated systems [12] that overcomes ill-conditioning of the Jacobian matrix. Based on the previous work [4], a new visual term preserving the so-called passivity-like property is proposed to improve the conditioning of the Jacobian matrix in the neighborhood of the desired position. A nonlinear controller is then derived and implemented on an experimental flying robot developed by the CEA. The experimental result show good performance and robustness of the proposed control strategy.

ACKNOWLEDGMENT

This work has been supported by the French company "WANY Robotics www.wanyrobotics.com " within the framework of a CEA-WANY Phd grant and a CNRS PICS grant (France-Australia).

REFERENCES

- [1] Altug, E., Ostrowski, J., & Mahony, Control of a quadrotor helicopter using visual feedback. In: *Proceedings of the IEEE international conference on robotics and automation, ICRA2002*.
- [2] R. L. Andersson. *A Robot Ping-Pong Player: Experiment in Real-Time Intelligent Control*. MIT Press, Cambridge, MA, USA, 1988.
- [3] Astolfi, A., Hsu, L., Netto, M., & Ortega, R., Two solutions to the adaptive visual servoing problem. *IEEE transactions on robotics and automation*, Vol.18(3), 2002, 387–392.
- [4] O. Bourquardez, R. Mahony, T. Hamel, F. Chaumette. *Stability and performance of image based visual servo control using first order spherical image moments*. In IEEE/RSJ Int. Conf. on Intelligent Robots and Systems, IROS'06, Beijing, China, Octobre 2006.
- [5] A. Castano and S. Hutchinson. Visual compliance: Task directed visual servo control. *IEEE transactions on Robotics and Automation*, 10(3):334–341, June 1993.

- [6] F. Chaumette. Potential problems of stability and convergence in image-based and position-based visual servoing. In *The Confluence of Vision and Control*, LNCIS, No. 237 pp. 66-78, 1998.
- [7] P. I. Corke and S. A. Hutchinson. A new partitioned approach to image-based visual servo control. In *Proceedings of the International Symposium on Robotics*, Montreal, Canada, May 2000.
- [8] P. I. Corke and S. A. Hutchinson. A new hybrid image-based visual servo control scheme. IEEE Int. Conf. on Decision and Control, CDC'2000, Sydney, Australia, December 2000.
- [9] K. Deguchi. Optimal motion control for image-based visual servoing by decoupling translation and rotation. In *Proceedings of the International Conference on Intelligent Robots and Systems*, pages 705–711, 1998.
- [10] B. Espiau, F. Chaumette, and P. Rives. A new approach to visual servoing in robotics. *IEEE Transactions on Robotics and Automation*, 8(3):313–326, 1992.
- [11] C. Fermuller, Y. Aloimonos. Observability of 3D motion. *Int. Journal of Computer Vision*, 37(1):43-64, June 2000.
- [12] T. Hamel and R. Mahony. Visual servoing of an under-actuated dynamic rigid-body system: An image based approach. *IEEE Transactions on Robotics and Automation*, 2002, Vol. 18(2), pages: 187-198.
- [13] S. Hutchinson, G. Hager, and P. Corke. A tutorial on visual servo control. *IEEE Transactions on Robotics and Automation*, 12(5):651–670, 1996.
- [14] K. P. Khosla, N. Papanikolopoulos, and B. Nelson. Dynamic sensor placement using controlled active vision. In *Proceedings of IFAC 12th World Congress*, pages 9.419–422, Sydney, Australia, 1993.
- [15] M. Lei and B. K. Ghosh. Visually guided robotic motion tracking. In *Proceedings of the thirteenth Annual Conference on Communication, Control and Computing*, pages 712–721, 1992.
- [16] Mahony R., Hamel T. et Chaumette F. *A Decoupled Image Space Approach to Visual Servo Control of a Robotic Manipulator*. Dans International conference IEEE, Robotics and Automation ICRA'2002, pp 3781-3786.
- [17] E. Malis, F. Chaumette, and S. Boudet. 2-1/2-d visual servoing. *IEEE Transactions on Robotics and Automation*, 15(2):238–250, April 1999.
- [18] G. Morel, T. Liebezeit, J. Szwedczyk, S. Boudet, and J. Pot. *Explicit incorporation of 2D constraints in vision based control of robot manipulators*, volume 250 of *Lecture Notes in Control and Information Sciences*, pages 99–108. Springer-Verlag, New York, USA, 1999. Edited by P. Corke and J. Trevelyan.
- [19] N. Papanikolopoulos, P. K. Khosla, and T. Kanade. Adaptive robot visual tracking. In *Proceedings of the American Control Conference*, pages 962–967, 1991.
- [20] J. A. Piepmeyer. *A dynamic quasi-newton method for model independent visual servoing*. Phd, Georgia Institute of Technology, Atlanta, USA, July 1999.
- [21] R. Pissard-Gibollet and P. Rives. Applying visual servoing techniques to control of a mobile hand-eye system. In *Proceedings of the IEEE International Conference on Robotics and Automation, ICRA'95*, pages 166–171, Nagasaki, JAPAN, 1995.
- [22] Shakernia, O., Ma, Y., Koo, T. J., & Sastry, S. Landing an unmanned air vehicle: vision based motion estimation and nonlinear control. *Asian journal of control*, 1(3), 128–146.
- [23] B. Yoshimi and P. K. Allen. Active, uncalibrated visual servoing. In *Proceedings of the IEEE International Conference on Robotics and Automation, ICRA'94*, pages 156–161, San Diego, CA, USA, 1994.
- [24] Zergeroglu, E., Dawson, D., de Queiroz, M., & Nagarkatti, S. Robust visual-servo control of robot manipulators in the presence of uncertainty. In: *Proceedings of the 38th conference on decision and control, CDC1999*.